NON-DESTRUCTIVE INCLUSION DETECTION AND QUANTIFICATION FOR CARBON FIBER LAMINATED COMPOSITES WITH PULSE-ECHO ULTRASONICS

John Moreton and David Jack

Baylor University

Abstract

Woven carbon fiber composites have desirable properties for many applications due to their high strength to weight ratio and thermal dimensionality, however many classical methods for inspection are not sufficient for damage detection and quantification. Due to the banded nature of the composite lamina, defects often occur between lamina and are not identifiable by standard visual methods. This may result in unexpected or premature failure. Similarly, assuming a part is damaged and overestimating the damage zone may result in parts being replaced unnecessarily. In this study a focused ultrasound transducer was used to detect a 3 micron thick sheet of Polytetrafluoroethylene (PTFE) placed between carbon fiber lamina. The scans were performed in a grid pattern, also known as a c-scan. Features in the time domain and the frequency domain are extracted for classification, as well as a newly developed block correlation method. The results presented in the paper highlight the various features and a discussion is presented of the advantages and disadvantages of the various techniques implemented to identify the defect.

Background and Requirements

Carbon fiber reinforced composites (CFRC) have been used in the aerospace industry for many years because of their desirable properties. In recent years they have also been used in various applications in the automotive industry and their usage is rapidly increasing (see e.g., [1]). Laminated composites offer particular challenges in quality control, damage evaluation/repair and inspection because many issues that occur at the interface between individual lamina cannot be seen from the surface. Also in certain applications features are purposefully [2] and inadvertently [3] inserted between carbon fiber layers that are neither carbon fiber nor resin. These features are termed foreign objects (FO) in the present paper. A variety of nondestructive testing techniques have been developed for inspection including pulse thermography, x-ray, MRI, ultrasound and others. Ultrasound in many applications is useful due to its portability, versatility, and relatively low infrastructure costs (see e.g., [4]). The outcome of an ultrasonic scan is a compilation of individual a-scans forming a complete c-scan for later analysis (see e.g., [4]). An a-scan represents the received acoustic wave from a single pulse of the transducer at a single location on a part. The c-scan is classically identified as some form of the signal intensity at a specific depth within the part for all of the a-scans across the part. The c-scan is often interpreted in a spatial x-y surface plot with contours of signal intensity corresponding to a specific depth within the part.

There are a series of papers that use Artificial Neural Networks (ANNs) (see e.g., [5]–[8]) to aid in defect characterization. Recently work in the use of tensor based analysis methods incorporating all of the a-scan signal [9] and statistical Bayesian methods [10] have also shown promise.

ANNs have been used for signal classification of the resulting waveform of an ultrasonic a-scan in a variety of studies. Several authors have used ANNs to analyze features of CFRCs.

Anastassopoulos *et al*. [5] compare several classification techniques, including multiple trained ANNs, and they highlight the ability of the ANNs to distinguish different thin film foreign objects (FO) placed between layers in a unidirectional CFRC. D'Orazio *et al.* [6] developed new preprocessing techniques of the captured acoustic waveform, that normalized length of waveform for parts of different thickness by removing data below a certain threshold. After preprocessing an ANN was used to analyze FOs in unidirectional CFRC, and they successfully identified defects in parts of different thickness than were given in the training data. Leo *et al.* [7] developed a new preprocessing technique, which used empirical mode decomposition to assist in feature extraction and then tested it with an ANN. Barry *et al.* [8] tested different ANN training algorithms with three different sets of input features to determine which were most robust in handling situations not encountered in training data. Barry *et al.* placed defects at different depths within a thin laminate stack for the training of their ANN. They then exercised the network on thicker panels with overlapping FOs of different materials, and demonstrated that a gradient descent training algorithm with momentum best identified the defects.

While ANN techniques focus on classifying individual a-scan data, without regard to the location of the a-scan, the tensor based methods gather the a-scan at each spatial location for the analysis. Tensor based methods of ultrasound scans of defects in CFRC are more recent in development. These methods have been used for anomaly detection in many different contexts, including structural health monitoring, neuroscience and transportation systems (see Fanaee and Gama [11] for an extensive review on this topic). You *et al*. [9] used the Tucker3 decomposition method to determine PTFE FOs depth, size and location in a plain weave CFRC with FOs at multiple depths.

A-scan data artificially generated to approximate non-defective parts as well as a variety of different defects does not perfectly match up with actual signals (see e.g., [10]). To address this issue Chiachío *et al.* [10] used a Bayesian method for classifying defects from ultrasound waveform scan data. This method was then validated using both synthetically generated signals with noise and experimental data obtain from through transmission ultrasonic scans of a cross-ply carbon epoxy laminate with damage from impact tests as well as fatigue loading.

In this research FOs in woven CFRCs are scanned ultrasonically. Different features in both the time and frequency domains are extracted from the generated a-scans and their efficacies in classification are discussed. Although not addressed in the present study, these features could be used as inputs for an ANN. In a new technique a-scan data was blocked together in spatial regions and correlated to group areas that have similar scan data. Then a simple linear iterative clustering algorithm to outline the defect area. Based on the results presented, capturing the frequency spectrum of the signal gated near the plane of the defect was found to best identify the defect with a weighted percent error of 9.7%.

Experimental Set-Up

Part Manufacture

Woven carbon fiber composites were manufactured using the vacuum assisted resin transfer molding (VARTM) process depicted in Figure 1 using 3K tow carbon fiber 6 oz. fabrics with twill, plain and satin weaves purchased from ACP Composites and AME 6001 IMF-35 resin provided by Ashland activated with a MEKP catalyst. The five lamina composite was composed of alternating 0° twill, 45° plain and 30° satin lamina in a stack as [0/45/30/0/45]. One 3 micron thick Polytetrafluoroethylene (PTFE) 31x12mm rectangle was used to create a disbond defect similar to that of Barry *et al.* [8]. The PTFE piece was placed in the part between the 3rd and 4th lamina relative to the tooling surface that also serves as the scan surface. Figure 2 shows where the

defect was placed in the part, as well as the area scanned with a red box. (Note that the scan was taken with the current face down, so the weave is flipped). After the parts were bagged and a good vacuum seal was achieved the resin and catalyst were mixed and infused through the part by vacuum. The part was then cured according to manufacturer recommended cure cycle achieving a heat of 50°C.

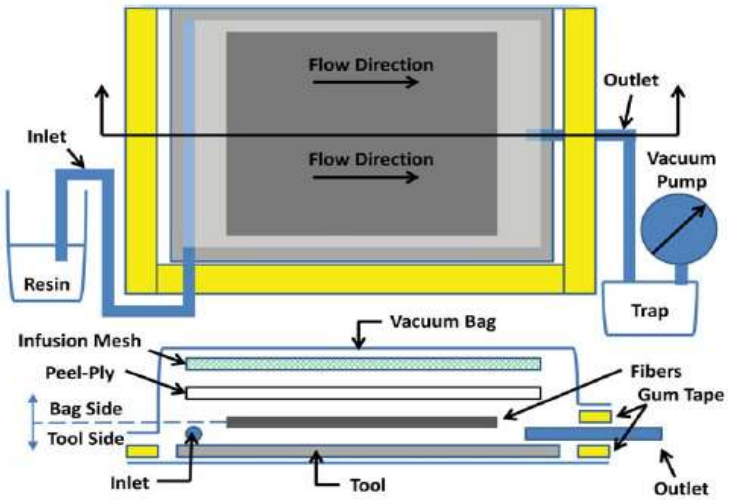

Figure 1: Diagram of VARTM process

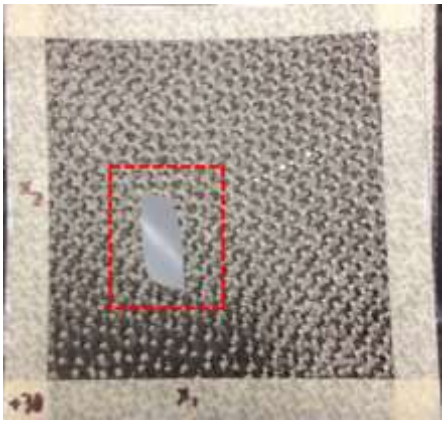

Figure 2: Defect and scan area on part

Scan Set-up

The part was scanned in a custom in-house fabricated water immersion scanning tank. A 15MHz spherical lens transducer from GE Oil and Gas Transducers with a focal point of 38.1 mm (1.5 inches) was used for pulse echo ultrasonic scanning. Data was taken at 160 MHz with 14 bit resolution using a US UltraTek EUT3160 pulser/receiver. All motor and pulser/receiver control and data acquisition was performed using an in-house developed custom Labview VI running on a standard Intel i7 desktop. In the present study we used a constant gain and did not include any results using distance amplitude correction. Two stepper motors with translation stages produced by Velmex are used to move the transducer following a predefined grid pattern (see Figure 3) with a spatial step size of 1/800 of a millimeter. All c-scan images provided in the following are for a

grid with 0.15 mm by 0.15 mm resolution. Special care is taken to insure that the part location relative to the coordinate system of the translation stages are in agreement. It is also very important that the part normal coincides with the direction vector of the transducer itself and this is accomplished by leveling the part and the stage to coincide in parallel planes to less than 0.4 mm. over the entire scan region.

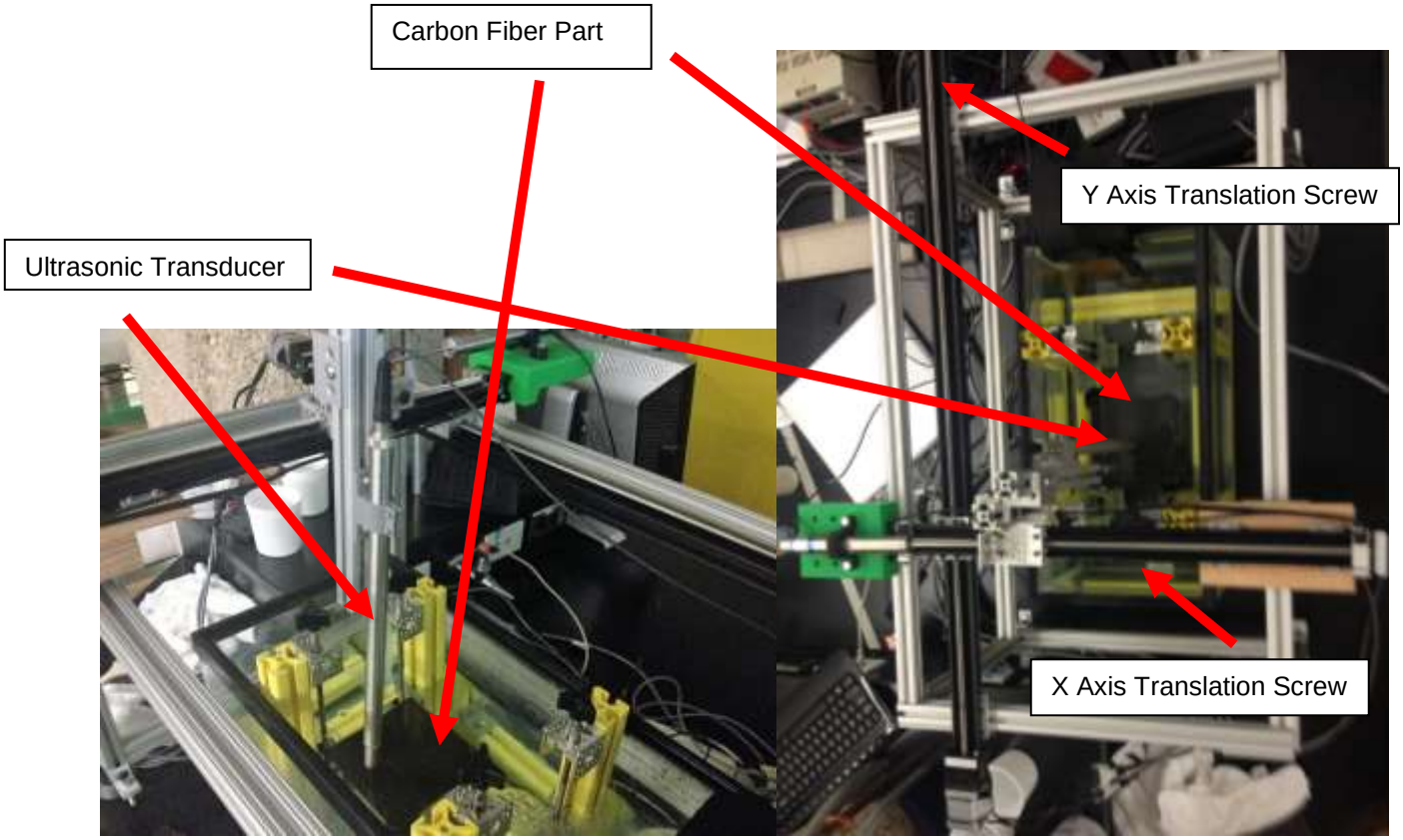

Figure 3: Custom ultrasonic Set-up.

Analysis Methods

Three major approaches of data analysis are used in this study and the differences between the effectiveness of the methods are discussed. First, time domain features were extracted from individual a-scans. Secondly, a blocked correlation method combined with image processing techniques were used to classify whether areas of the part are defective or not. Finally, frequency domain features were taken from the back wall of individual a-scans.

Time Domain Features

Figure 4 contains a typical a-scan taken from a region known to not contain a defect (left) and a typical a-scan from the region known to contain the defect (right). The a-scan is the signal intensity returned from a single firing of the transducer operating in pulse-echo mode. In classical a-scans of homogeneous parts the first peak corresponds to the front wall of the part whereas the second peak would be the back-wall of the part. As the parts scanned in the present study are woven laminates, there are many internal echoes due to the presence of multiple regions of inhomogeneity corresponding to pure resin regions and regions that have a fiber tow infused with

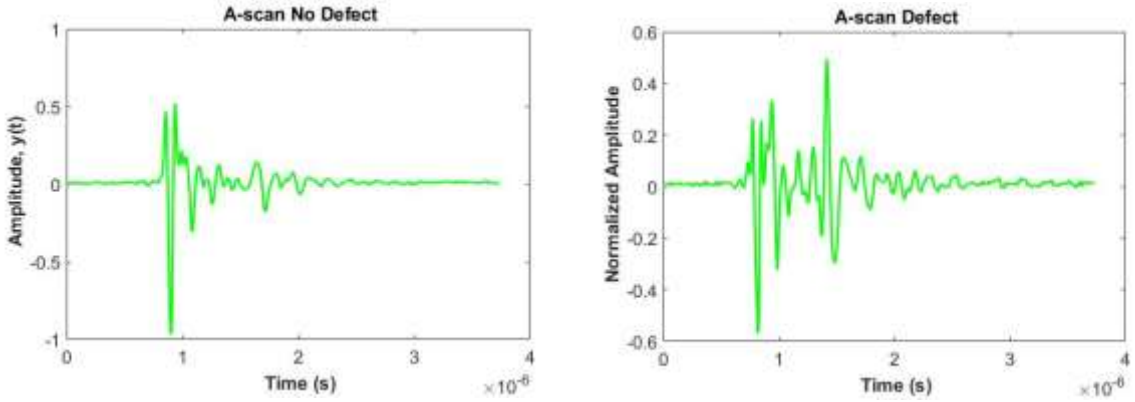

Figure 4: Two Example A-scans

resin. Thus the signal returned to the transducer contains not only the front and back wall echoes, but the echoes of individual fiber tows thus complicating the analysis. Note, that for lower frequency transducer systems, (such as that of [5], [6], [8]) the gap between tows may be below the signal detection threshold and thus the internal echoes between lamina may be less prevalent in the a-scans. But the higher frequency systems are necessary for investigating the individual tow features (see e.g., [12]–[14]). In the present study, we maintain the focus on the higher frequency systems to retain the ability to capture the individual lamina microstructure as required for quantifying the individual ply orientation information [14]. Based on earlier works, the use of a lower frequency system will allow for the easier detection of the FO within the part.

For the time analysis, the initial front wall aspect of the signal is removed and the focus is only

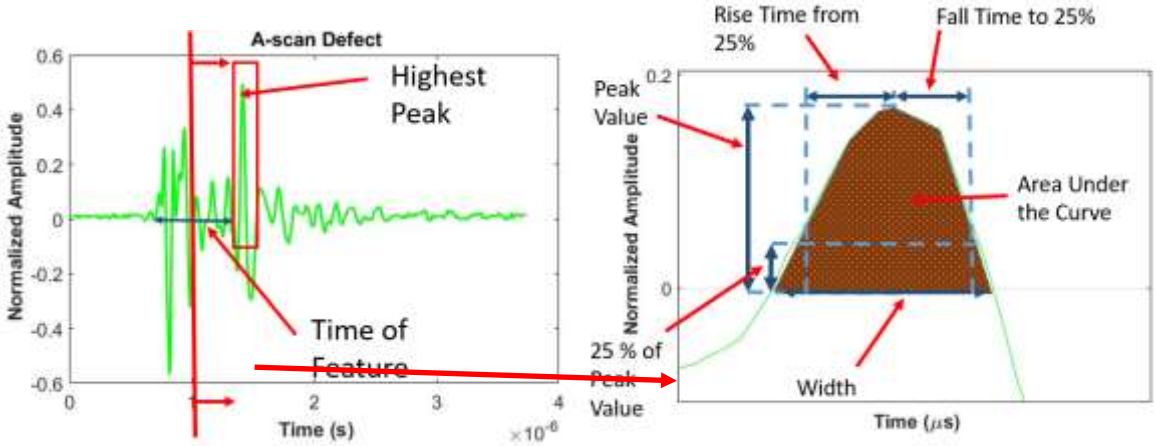

Figure 5: Peak Feautures

on the latter portion of the signal. In Figure 5, the signal prior to 1 microsecond is discarded. There are a variety of features in the latter portion of the signal that may be useful in identifying the presence of a foreign object as highlighted in the zoomed in region of Figure 5. Several aspects of interest in the present study are the time when the highest peak occurs as this is assumed to either be the back wall or the foreign object itself. A second feature of interest is the duration of time between the beginning and end of this peak, defined as the time when the intensity crosses the time axis. The time integral of this peak can be related to signal intensity, and it is thought that the foreign object may reflect more sound energy than would that of the normal interlaminar boundaries. The time integral is determined by applying a hybrid Simpson's 1/3 and 3/8 rules to the peak curve to approximate the area. Another feature that can be used to identify the FO is the rise time, and in the present study it was found that the rise time from 25 percent of the signal intensity to the signal peak avoided issues of interlaminar echoes and system noise. Similarly the fall time to 25 percent was investigated, and is defined as the time between the top of the peak and the time when the intensity is 25 percent of the peak. The final feature investigated is termed the time of feature and this represents the duration of time between the front wall of the part and the beginning of the highest peak. This last feature to study is also useful in identify the depth of the FO within the laminate once the location of the feature is identified.

Block Correlation Method

A method to post-process the results from the various features within the a-scans is a block correlation method. In this method, a group of signals near a specific location is compared to that of the bulk average. This is done by first creating the average a-scan of the entire part by summing all of the a-scans. This representative a-scan is shown in Figure 6 as compared to the individual a-scan at a single point as shown in Figure 5. This average a-scan was generated after first shifting the time axis so that the front wall of the part, indicated by the onset of the signal from an individual a-scan, is at the same time over the entire surface. This time is redefined as $t = t_{front} = 0$. From this averaged a-scan the times of local maxima and minima of the representative scan are determined. These times are referred to as the peak times. The representative a-scan has significantly less noise than a single a-scan and retains a back wall echo as well as echoes for the layers. Unfortunately this averaged a-scan loses the subtle spatial features due to the weave patterns within the composite. The plane of the part is then divided into a grid pattern, where each square is larger than the weave pattern within the individual lamina. Then all of the a-scans associated with an individual area were added together to create a combined scan representative of that block. The signal intensity of the representative a-scans at each of the peak times for the overall representative a-scan are correlated with each other using the Pearson correlation coefficient, then a threshold is used to group these blocks together. Figure 8 represents each block as a circle and each color represents a group of blocks well correlated with each other.

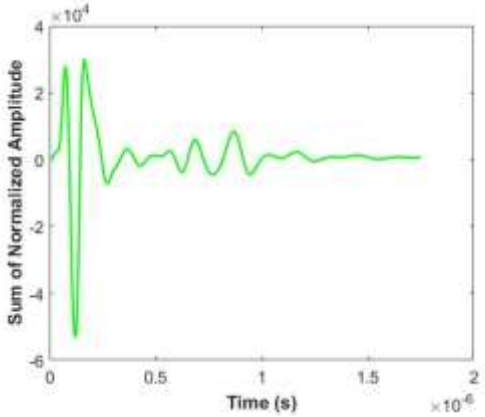

Figure 6: A-scan Summation

Since the rectangles represented by the block method do not give good resolution and do not match up with irregular shape further analysis must be done. In the image processing toolbox of MATLAB there is a function which segments an image into regions with similar values called superpixels using a simple linear iterative clustering algorithm.[15] Each superpixel is assigned to a group based on the group of blocks that overlaps it the most. Then the group covering the largest area is classified as non-defective and rest of the groups are classified as defective.

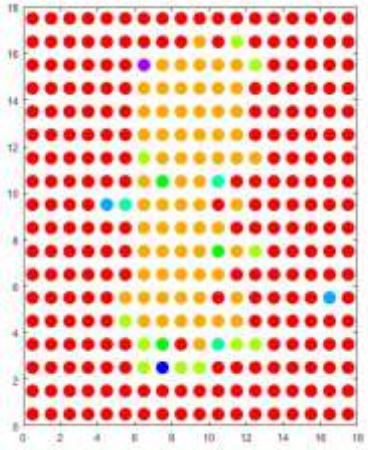

Figure 7: Correlated Blocks

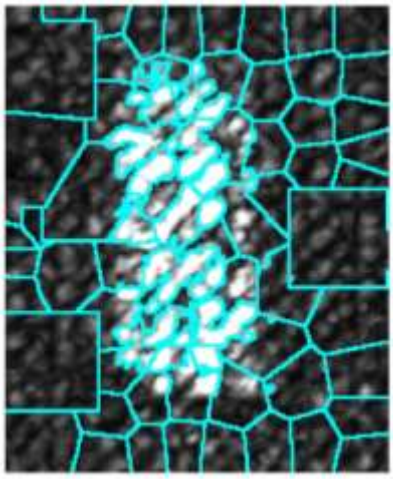

Figure 8: Superpixels superimposed over C-scan Image

Frequency Domain Features

A discrete Fourier reconstruction is performed on data taken from a .5 μs gate taken shortly after the depth that the defect is identified to be at from the time analysis. One feature that was extracted for classification was the frequency with the maximum amplitude. The Fourier reconstruction of the individual Fourier coefficients is then converted to a discretized density function then the skewness was calculated using

$$S = \frac{\frac{1}{n} * \sum_{i=1}^{n} (x_i - \bar{x})^3}{\left(\frac{1}{n} * \sum_{i=1}^{n} (x_i - \bar{x})^2\right)^{3/2}} \quad (1)$$

and kurtosis using

$$K = \frac{\frac{1}{n} * \sum_{i=1}^{n} (x_i - \bar{x})^4}{\left(\frac{1}{n} * \sum_{i=1}^{n} (x_i - \bar{x})^2\right)^{2}} \quad (2)$$

Where S is the skewness, n is the total number of points, x_i is the ith point and $\bar{x}$ is the mean the data and K is the kurtosis. In the present study, the coefficient x_i corresponds to the amplitude of the signal intensity contribution from a given frequency.

Figure 9 shows an example of the resulting frequency spectrum from the discrete Fourier transform for both the defective area and the non-defective area. The dominate peaks are in similar location in the frequency spectrum, but the dominate peaks are both much stronger for the scan over the defect relative to that of the scan from the non-defective region.

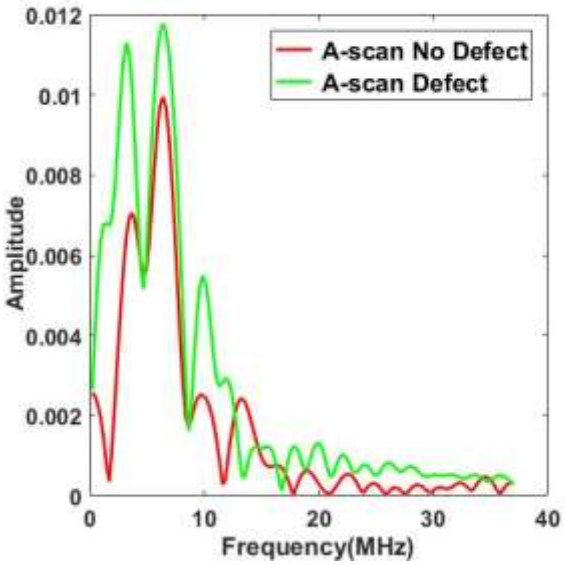

Figure 9: Example Fourier Transforms

Post-Processing

After the values from each of the three aforementioned methods categories were obtained for each of the individual a-scans, the data was classified into two groups, defect or non-defect. This was done using a user variable threshold can be manually adjusted until the highest contrast image was obtained. The classified data at each individual spatial location is smoothed by comparing the classification to that of the nearest neighbors and changing it if more than a certain threshold percentage of them are different. In this study the threshold value is determined by minimizing the error based on the known size of the defect.

Results and Conclusions

Time Domain

Based on the investigated results it was determined that one of the better features for classifying the a-scans in the time domain was the intensity obtained from the peak value of the a-scan after the initial front wall echo. Figure 10 shows an example of the final classification based on the peak amplitude in the time domain. The area inside the dashed line represents the known size, and shape of the defect, but location of the dashed line is made visually by best matching the results of the data. The white area represents places classified as defective and the black represents areas classified as non-defective. Using the results from the signal peak value does a very reasonable job in identifying the defect as a defect; however, it also classifies

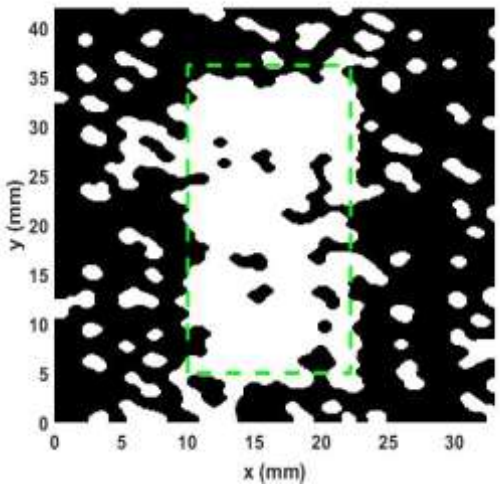

Figure 10: Peak Value Classification

many non-defective areas as defective. The misclassified areas are in a pattern that is very similar to that of the twill weave, which makes sense due to the high frequency of the transducer used. The effectiveness of the classification can be quantified in a confusion table as well as with percent error values. The confusion table divides that data based on the category it is placed in and the actual category. In a confusion table the columns correspond to the correct category and the row represents the category the method classified the points. A perfect result would only have non-zero values on the diagonal. The confusion table for the peak value of the signal intensity is shown in Table I.

Table I: Confusion Table for Peak Value

	Defective	Non- Defective
Classified as Defective	21.9%	16.2%
Classified as Non-Defective	4.1%	57.8%

There are several ways to interpret the confusion table depending upon the objective from the analysis. One method is the percent error defined as the total incorrectly classified points divided by the total number of points (see e.g. [7])

$$\%\ Error = 100 * \frac{Total\ \#\ of\ Incorrect\ Point}{Total\ \#\ of\ Points} \tag{3}$$

Thus from table the $\%\ Error$ is equal to 4.1%+16.2% = 20.3%. However, incorrect classifications can be divided into two kinds: Type 1) a point is incorrectly classified as defective: (see e.g. 7)

$$Type\ 1\ \%\ Error = 100 * \frac{\#\ of\ Non-Defective\ Points\ Incorrect}{\#\ of\ Non-Defective\ Points} \tag{4}$$

Type 2) a point is incorrectly classified as non-defective: (see e.g. 7)

$$Type\ 2\ \%\ Error = 100 * \frac{\#\ of\ Defective\ Points\ Incorrect}{\#\ of\ Defective\ Points} \tag{5}$$

Thus from Table 1, the $Type\ 1\%\ Error$ is 16.2/(57.8+16.2) = 21.9% and the $Type\ 2\%\ Error$ is 4.1/(21.9+4.1) = 15.9%. A composite of the percent error of each of these is robust against the size of the relative sizes of the defective region and non-defective region.

$$Weighted\ \%\ Error = 100 * \frac{Type\ 1\% + Type 2\%}{2} \tag{6}$$

For the data from the confusion table in Table 1, this will yield a combined error of (21.9+15.9)/2 = 18.9%. Notice that the weighing can be shifted onto one or the other parameter by biasing one error type over the other. Equation 6 defines the relative importance of each type of error to be identical. Regardless, the confusion table is a mechanism for quantifying the accuracy of the detection technique used and there are a variety of mechanisms to define the error.

The various percent errors for each of the aforementioned time domain features are shown in Table II. Based on the results in Table 2 it is clear that the identification of the location of the

defect is very good as seen by the low values of the Type 2 error, whereas there are many false positives for a defect in a non-defective region as seen by the high value of the Type 1 error. If one only was concerned with the identification of the defect than the time of feature and the width are the two best indicators, but they lend themselves to many false positives, and thus the overall best methods that balance the defect identification while limiting the number of false positives are the Area and the Peak Value identification methods as seen by their low values for the Weighted Percent Error.

Table II: Time Domain Percent Error

	Overall Percent Error	Type I Percent Error	Type 2 Percent Error	Weighted Percent Error
Area	20.3	22.7	13.5	18.1
Peak Value	20.3	21.9	15.9	18.9
Width	36.6	46.8	7.6	27.2
Rise Time	37.2	43.9	18.3	31.1
Time of Feature	55.5	73.1	5.3	39.2
Fall Time	35.9	19.1	83.8	51.5

Block Correlation Method

The final classified c-scan for the block correlation method is shown in Figure 11. The generated superpixels do not give a sharp pattern of the image because they are also outlining the weave and the blocks do not match up perfectly where they overlap the border of the defect. However, away from the edges of the defect this method is accurate with almost no false positives. This method has the second best weighted percent error as seen in Table 3.

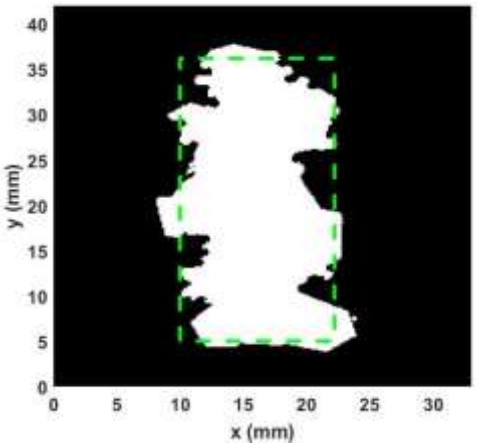

Figure 11: Block correlation classification

Table III: Block Correlation Percent Error

	Overall Percent Error	Type I Percent Error	Type 2 Percent Error	Weighted Percent Error
Correlation	8.5	3.5	22.6	13.1

Frequency Domain

The final set of results is for the feature identification from the frequency spectrum. Based on the results investigated, the skewness gave the best results of any of the features extracted. It has small areas inside both the defective area and non-defective area that were just dense enough to resist the image smoothing as seen in the regions of Figure 12 where there is no known defect. Regardless, from Figure 12 the original size and shape of the rectangular defect can be identified clearly.

In the frequency domain the skewness outperformed the kurtosis and the frequency of the maximum amplitude as shown by the percent error computed from the confusion tables and given in Table 4. Each one of the methods yielded similar levels of Type I error, thus very few false-positives for defect identification. The difference between the investigated features is composed primarily by Type II error. The frequency plot at each location, similar to those of Figure 9, tends to have a dominant peak in regions with no defect, whereas the largest two peaks are much closer in size in the defect region, the location of the two peaks is close to the peak in the non-defective region, so the location of the frequency with maximum amplitude does not discriminate as well as shape related factors such as skew and kurtosis. Each one of the frequency features benefitted significantly from the image processing, which smooths out differences that appear to come from the subtle weave pattern as shown in Figure 8. The skewness classified the frequency spectrum data better because the skewness is effected by the direction data differs from the mean because it takes an odd power of the deviations(eqn 1) whereas the kurtosis takes an even power (eqn 2) and the right tail tends to me longer than the left. Thus the kurtosis would not be able to differentiate if data is biased above or below the mean, whereas the skewness may indicate whether the date biases above or below the centroid.

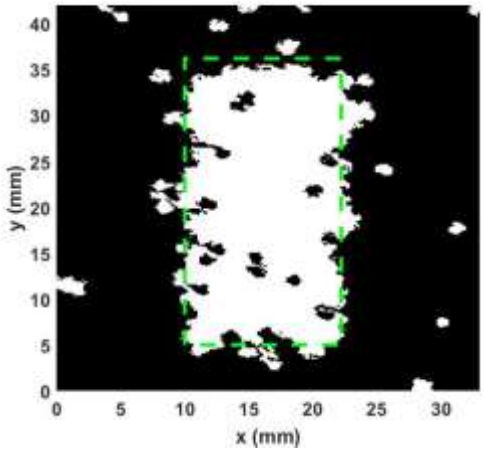

Figure 12: Skewness classification

Table IV: Frequency Domain Percent Error

	Overall Percent Error	Type I Percent Error	Type 2 Percent Error	Weighted Percent Error
Kurtosis	11.6	5.2	29.8	17.5
Skewness	7.5	5.1	14.2	9.7
Frequency of Max. Amplitude	21.1	6.4	62.9	34.6

Conclusion

In this paper different methods for identifying the location of a foreign object (FO) within a carbon fiber reinforced composite were compared. A CFRC part with an FO was fabricated and scanned. Three methods were used to classify a-scan data as either defective or non-defective. The skewness of the discrete Fourier transform of the time after the defect was found to be the most effective method investigated with a weighted percent error of just under 10%. This low error is even more impressive considering the large scatter of the wave within the sample due to the variations of the geometry within the woven lamina themselves. The new block and correlate method was next best with a weighted percent error of 13.1%. The time domain features were the least effective, with weighted percent errors ranging from 18.1%-51.5%.

Acknowledgements

The authors would like to thank L-3 for their generous support of our research and for the resin provided by Ashland. The authors also thank Nate Blackman, a graduate research assistant at Baylor University, for his work on the LabVIEW VI for the ultrasonic scanner.

References

[1] D. S. Mazumdar, “How to win in carbon composites for the automotive market.” [Online]. Available: http://www.compositesworld.com/columns/how-to-win-in-carbon-composites-for-the-automotive-market. [Accessed: 07-Jul-2017].

[2] N. Takeda and S. Minakuchi, “Optical fiber sensor based life cycling monitoring and quality assessment of carbon fiber reinforced polymer matrix composite structures,” in *2017 25th Optical Fiber Sensors Conference (OFS)*, 2017, pp. 1–4.

[3] R. A. Smith, “Composite defects and their detection,” *Encyclopedia of Life Support Systems*, vol. 3. pp. 103–143, 2009.

[4] L. W. Schmerr Jr, *Fundamentals of Ultrasonic Nondestructive Evaluation: A Modeling Approach*, 1998 edition. New York: Springer, 1998.

[5] A. A. Anastassopoulos, V. N. Nikolaidis, and T. P. Philippidis, “A comparative study of pattern recognition algorithms for classification of ultrasonic signals,” *Neural Comput. Appl.*, vol. 8, no. 1, pp. 53–66, 1999.

[6] T. D’Orazio, M. Leo, A. Distante, C. Guaragnella, V. Pianese, and G. Cavaccini, “Automatic ultrasonic inspection for internal defect detection in composite materials,” *NDT E Int.*, vol. 41, no. 2, pp. 145–154, Mar. 2008.

[7] M. Leo, D. Looney, T. D’Orazio, and D. P. Mandic, “Identification of Defective Areas in Composite Materials by Bivariate EMD Analysis of Ultrasound,” *IEEE Trans. Instrum. Meas.*, vol. 61, no. 1, pp. 221–232, Jan. 2012.

[8] T. Barry, M. Kesharaju, C. Nagarajah, and S. Palanisamy, “Defect characterisation in laminar composite structures using ultrasonic techniques and artificial neural networks,” *J. Compos. Mater.*, vol. 50, no. 7, pp. 861–871, Mar. 2016.

[9] R. You, Y. Yao, and J. Shi, “Tensor-based ultrasonic data analysis for defect detection in fiber reinforced polymer (FRP) composites,” *Chemom. Intell. Lab. Syst.*, vol. 163, pp. 24–30, Apr. 2017.

[10] J. Chiachío, N. Bochud, M. Chiachío, S. Cantero, and G. Rus, “A multilevel Bayesian method for ultrasound-based damage identification in composite laminates,” *Mech. Syst. Signal Process.*, vol. 88, pp. 462–477, May 2017.

[11] H. Fanaee-T and J. Gama, “Tensor-based anomaly detection: An interdisciplinary survey,” *Knowl.-Based Syst.*, vol. 98, pp. 130–147, Apr. 2016.

[12] S. Stair, D. Jack, and J. Fitch, “CHARACTERIZATION OF CARBON FIBER LAMINATES: DETERMINING PLY ORIENTATION AND PLY TYPE VIA ULTRASONIC A-SCAN AND C-SCAN TECHNIQUES,” presented at the SPE ANTEC, Las Vegas, 2014, pp. 535–539.

[13] S. Stair, “Ultrasonic Characterization of Fiber Reinforced Composites,” presented at the SPE ACCE, Novi, MI, 12-Sep-2013.

[14] D. Jack, J. Fitch, and T. Vo, “Method and Sytem of Non-Destructive Testing for Composites,” Patent filing 14/386,449

[15] R. Achanta, A. Shaji, K. Smith, A. Lucchi, P. Fua, and S. Süsstrunk, “SLIC superpixels compared to state-of-the-art superpixel methods,” *IEEE Trans. Pattern Anal. Mach. Intell.*, vol. 34, no. 11, pp. 2274–2282, 2012.